IEEE Access
Multidisciplinary | Rapid Review | Open Access Journal

Received June 20, 2021, accepted July 19, 2021, date of publication July 26, 2021, date of current version September 17, 2021.

Digital Object Identifier 10.1109/ACCESS.2021.3099430

A Transformed Coprime Array With Reduced Mutual Coupling for DOA Estimation of Non-Circular Signals

FENGTONG MEI, HAIYUN XU, WEIJIA CUI, BIN BA, AND YINSHENG WANG
National Digital Switching System Engineering and Technological Research Center, Zhengzhou 450001, China
Corresponding author: Haiyun Xu (xuhaiyun1995@163.com)

This work was supported in part by the National Natural Science Foundation of China under Grant 61401513.

ABSTRACT Recently, the design of sparse linear array for direction of arrival (DOA) estimation of non-circular (NC) signals has attracted great attention because the difference and sum co-array offered by non-circularity increases the aperture of virtual linear array. In this paper, we present a coprime array with shifted and flipped sub-array for the DOA of non-circular signals. By shifting one sub-array, the proposed array structure achieves a higher number of consecutive lags than the prototype coprime array with the same number of sensors. Then, through flipping the shifted sub-array with the zero point as the symmetry point, the number of sensor pairs with small separation is significantly reduced, making the resulting structure much sparser. For the proposed array structure, we derive the closed-form expression for the number of consecutive lags, the optimal distribution of two sub-arrays with a given number of sensors and the weight function. Numerical simulations are conducted to verify the superiority of the proposed array over the existing sparse arrays.

INDEX TERMS Coprime arrays, direction of arrival (DOA), non-circular signal, degree of freedom, mutual coupling.

I. INTRODUCTION

Direction-Of-Arrival (DOA) estimation is one of the important research fields in array signal processing [1]–[3]. For uniform linear array (ULA), the traditional estimation method such as multiple signal classification (MUSIC) [4] and estimation of signal parameters via rotational invariance techniques (ESPRIT) [5] can only resolve $M-1$ sources under the condition of M physical sensors. However, the underdetermined conditions where the number of target sources is larger than that of array sensors are very common in the real world.

To solve this problem, many sparse array structures have been proposed to increase the degrees of freedom (DOFs). The minimum redundant array (MRA) [6] is a well-known sparse array that maximizes the number of consecutive lags based on difference co-array. However, as the closed-form expression of the configuration of MRA does not exist, it is difficult for array design. The nested arrays (NA) [7] and coprime arrays (CPA) [8] are the most notable sparse arrays presented recently. They both consist of two uniform linear arrays, making it possible to express their structures analytically. Based on them, many underdetermined DOA estimation approaches have been proposed, such as spatial smoothing subspace MUSIC (SS-MUSIC) [9] and compressed sensing algorithm [10], [11] [12]. In [13], coprime arrays with compressed inter-element spacing (CACIS) and coprime arrays with displaced sub-arrays (CADiS) are proposed, which reveals that the proper displacement of subarrays and inter-element spacing can increase the DOFs and improve estimation accuracy.

However, many of the sparse array design schemes do not consider the effect of mutual coupling. Therefore, the DOA estimation performance will drop sharply when this effect is strong. To tackle this problem, the super nested arrays (SPNA) are designed by rearranging the dense ULA part of a nested array in [14]. In this way, the number of small inter-element spacing can be decreased to reduce the mutual coupling effect, while the key advantages of the nested array can be maintained. In [15], the augmented nested array (ANA) is introduced. It is obtained by splitting the dense uniform linear array part in the nested array and placing them on both sides of the sparse uniform array

The associate editor coordinating the review of this manuscript and approving it for publication was Brian Ng.

of the nested array. Compared with SPNA, it can provide a higher DOFs and reduce the mutual coupling effect. In [16], a new sparse array named the maximum inter-element spacing constraint (MISC) is proposed, consisting of three sparse ULAs plus a ULA with two sensors. Comparing to the SPNA and ANA, it has a sparser structure and a higher DOFs.

However, the above sparse arrays are designed using the covariance matrix without considering the NC characteristic of signal. NC signals are frequently encountered in digital communications, such as binary phase shift keying (BPSK) and Unbalance Quadrature PSK (UPSK). Compared with circular signals, NC signals can provide more information for DOA estimation because their elliptic covariances are not equal to zero [17]–[26]. In addition, the researchers also introduce elliptic covariance in the process of sparse array design to improve the performance of DOA estimation. In [27], the difference and sum (diff-sum) co-array is proposed, and the prototype coprime array [8] is taken as a model to verify the performance advantage of the diff-sum co-array. In [28], a diff-sum coprime array with multiperiod sub-arrays (DsCAMpS) is designed, making a substantial increase in DOFs. In [29], the nested array with displaced sub-array (NADiS) is designed for NC signals by placing the two subarrays side by side. It has a similar array structure to the nested array but provides larger physical and virtual array aperture. In [30], the transformed nested array (TNA-I) is designed by swapping positions of the two sub-arrays of the nested array. Then, TNA-II is proposed by splitting the dense sub-array of TNA-I into two parts, yielding a higher DOFs than the above arrays. However, these arrays for NC signals do not consider the mutual coupling effect, resulting in performance degradation when this effect is strong. Hence, in [31], the improved coprime array is designed by flipping one sub-array of a coprime array with zero point. It reduces mutual coupling for the DOA estimation of NC signals. However, it does not increase the DOFs compared with the prototype coprime array, so that further improvement is possible.

In this paper, we propose a shifted coprime array by shifting one sub-array of the coprime array to increase the DOFs for the DOA estimation of NC signals. Then, flipping it with zero-point as a symmetry point, the coprime array with shifted and flipped sub-array (CASFS) is obtained. Our contributions are summarised as follows:

1) The closed-form expressions for the physical sensor location and the number of consecutive lags are derived, and the optimal distribution of sensors to each sparse ULA is also given. Compared with the existing coprime array family, the proposed array can provide a higher DOFs and a larger physical array aperture.

2) For the proposed array, we derive the weight functions and prove that the weight functions with small values are less than the existing sparse arrays and even zero, which shows that the CASFS has a much sparser structure and can tolerate severer mutual coupling.

The rest of this paper is organized as follows: in Section II, the signal model is presented. Section III describes the novel sparse array structure and its properties. Section IV presents numerical examples; Section V summarises this paper.

Throughout this paper, we make use of the following notations. Matrices and vectors are represented by capital letters and lower letters in boldface, respectively. Given a matrix $\mathbf{A}$, we use $\mathbf{A}^T$, $\mathbf{A}^H$, and $\mathbf{A}^*$ to denote the transpose, the Hermitian transpose, and the conjugate of $\mathbf{A}$, respectively. We use $\otimes$ and $\odot$ to denote the Kronecker product and the Khatri-Rao product, respectively. The statistical expectation is denoted by $\mathbf{E}\{\cdot\}$, and $\mathbf{vec}\{\cdot\}$ is the vectorization operation. $gcd(m, n)$ represents the greatest common divisor between m and n. For two given sets of integers $\mathbb{X}$ and $\mathbb{Y}$, the summation set between $\mathbb{X}$ and $\mathbb{Y}$ is given by $sum(\mathbb{X}, \mathbb{Y}) = \{x + y | x \in \mathbb{X}, y \in \mathbb{Y}\}$ and their difference set is $diff(\mathbb{X}, \mathbb{Y}) = \{x - y | x \in \mathbb{X}, y \in \mathbb{Y}\}$. In addition, $\mathbb{X} + a$ represents $\{x + a | x \in \mathbb{X}\}$, where a is an integer.

II. PRELIMINARIES

A. SIGNAL MODEL

Considering a sparse linear array with Q physical sensors, the unit spacing equals half wavelength $\lambda/2$, denoted by d. The set of sensor positions is given by

$$\mathbb{L} = \{d_1, d_2, \ldots, d_Q\}d, \tag{1}$$

where d_q is an integer. Supposing there are K far-field uncorrelated, narrow-band sources denoted by $\mathbf{s}(t) = [s_1(t), s_2(t), \ldots, s_K(t)]^T$ impinging on the array from directions $\boldsymbol{\theta} = [\theta_1, \theta_2, \ldots, \theta_K]$, the steering vector at angle θ_k is,

$$\mathbf{a}(\theta_k) = [e^{j\beta_k d_1}, e^{j\beta_k d_2}, \ldots, e^{j\beta_k d_Q}]^T, \tag{2}$$

where $\beta_k = \pi \sin\theta_k$. We further assume that all signals are strictly non-circular and quasi-stationary with F frames and frame length T. $t \in \{1, 2, \ldots, T\}$.

Then the received data of the sparse array is given by

$$\mathbf{x}(t) = \sum_{k=1}^{K} \mathbf{a}(\theta_k)\bar{s}_k(t)e^{j\phi_k} + \mathbf{n}(t) = \mathbf{A}\boldsymbol{\Phi}\bar{\mathbf{s}}(t) + \mathbf{n}(t), \tag{3}$$

where $\mathbf{A} = [\mathbf{a}(\theta_1), \mathbf{a}(\theta_2), \ldots, \mathbf{a}(\theta_k)]$ is the $Q \times K$ array manifold matrix, $\bar{\mathbf{s}}(t) = [\bar{s}_1(t), \bar{s}_2(t), \ldots, \bar{s}_K(t)]^T$ is the $K \times 1$ real-valued signal vector, $\Phi = diag\{e^{j\phi_1}, e^{j\phi_2}, \ldots, e^{j\phi_K}\}$ and ϕ_k is the NC phase of the k-th signal. $\mathbf{n}(t) = [n_1(t), n_2(t), \ldots, n_Q(t)]^T$ represents the $Q \times 1$ noise vector corresponding to the t-th snapshot, where $n_q(t)$ is independent and identically distributed (i.i.d.) additive Gaussian noise with power σ_n^2 and it is independent of the sources. Then, the covariance matrix of the received signals can be expressed as

$$\mathbf{R}_\mathbf{x} = \mathbf{E}\{\mathbf{x}(t)\mathbf{x}(t)^H\} = \sum_{k=1}^{K} p_k \mathbf{a}(\theta_k)\mathbf{a}^H(\theta_k) + \sigma_n^2\mathbf{I}, \tag{4}$$

where $p_k = \mathbf{E}\{\bar{s}_k(t)\bar{s}_k(t)\}$ represents the power of the k-th signal, and the elliptic covariance matrix for the received

signals, due to the characteristic of NC signals, is not zero and given by

$$\mathbf{R}'_{\mathbf{x}} = \mathbf{E}\{\mathbf{x}(t)\mathbf{x}(t)^T\} = \sum_{k=1}^{K} \bar{p}_k \mathbf{a}(\theta_k)\mathbf{a}^T(\theta_k), \tag{5}$$

where $\bar{p}_k = \mathbf{E}\{\bar{s}_k(t)\bar{s}_k(t)e^{j2\phi_k}\}$. In order to make use of the benefits associated with NC signals, we construct an extended observation, given by

$$\mathbf{y}(t) = \begin{bmatrix} \mathbf{x}(t) \\ \mathbf{x}^*(t) \end{bmatrix} = \begin{bmatrix} \mathbf{A}\Phi \\ \mathbf{A}^*\Phi^* \end{bmatrix} \bar{\mathbf{s}}(t) + \begin{bmatrix} \mathbf{n}(t) \\ \mathbf{n}^*(t) \end{bmatrix}. \tag{6}$$

Then the covariance matrix of $\mathbf{y}(t)$ can be expressed as

$$\mathbf{R}_{\mathbf{y}} = \begin{bmatrix} \mathbf{R}_{\mathbf{x}} & \mathbf{R}'_{\mathbf{x}} \\ \mathbf{R}'^*_{\mathbf{x}} & \mathbf{R}^*_{\mathbf{x}} \end{bmatrix} = \widetilde{\mathbf{A}}\mathbf{P}\widetilde{\mathbf{A}}^H + \sigma_n^2\mathbf{I}_{2Q}, \tag{7}$$

where $\widetilde{\mathbf{A}} = [(\mathbf{A}\Phi)^T, (\mathbf{A}\Phi)^H]^T$, $\mathbf{P} = \mathrm{diag}\{p_1, p_2, \ldots, p_k\}$. Vectorizing $\mathbf{R}_{\mathbf{y}}$ yields

$$\mathbf{z} = \mathbf{vec}\{\mathbf{R}_{\mathbf{y}}\} = \mathbf{B}\mathbf{p} + \sigma_n^2\mathbf{i}, \tag{8}$$

where

$$\mathbf{B} = \widetilde{\mathbf{A}}^* \odot \widetilde{\mathbf{A}} \tag{9}$$

is called the equivalent array manifold of difference and sum co-array, $\mathbf{p} = [p_1, p_2, \ldots, p_k]^T$ and $\mathbf{i} = \mathbf{vec}(\mathbf{I}_{2Q})$.

B. DIFFERENCE AND SUM CO-ARRAY

Now, we focus on $\mathbf{B}$ to get more insight into it. From (9), we can obtain the k-th column of matrix $\mathbf{B}$, given by

$$\begin{aligned} \mathbf{b}(\theta_k) &= \widetilde{\mathbf{a}}^*(\theta_k) \otimes \widetilde{\mathbf{a}}(\theta_k) \\ &= \begin{bmatrix} \mathbf{a}^*(\theta_k)e^{-j\phi_k} \\ \mathbf{a}(\theta_k)e^{j\phi_k} \end{bmatrix} \otimes \begin{bmatrix} \mathbf{a}(\theta_k)e^{j\phi_k} \\ \mathbf{a}^*(\theta_k)e^{-j\phi_k} \end{bmatrix} \\ &= \mathbf{K}_{2Q,2} \otimes \mathbf{I}_M \bar{\mathbf{b}}(\theta_k), \end{aligned} \tag{10}$$

where $\mathbf{K}_{2Q,2}$ denotes a commutation matrix defined in [32] and $\bar{\mathbf{b}}(\theta_k)$ is given by [30]

$$\bar{\mathbf{b}}(\theta_k) = \begin{bmatrix} \mathbf{a}^*(\theta_k) \otimes \mathbf{a}(\theta_k) \\ \mathbf{a}(\theta_k) \otimes \mathbf{a}(\theta_k)e^{j2\phi_k} \\ \mathbf{a}^*(\theta_k) \otimes \mathbf{a}^*(\theta_k)e^{-j2\phi_k} \\ \mathbf{a}(\theta_k) \otimes \mathbf{a}^*(\theta_k) \end{bmatrix}, \tag{11}$$

indicating that $\mathbf{b}(\theta_k)$ and $\bar{\mathbf{b}}(\theta_k)$ have the same elements, but the order is different. By analyzing (11), we find that $\mathbf{a}^*(\theta_k) \otimes \mathbf{a}(\theta_k)$ corresponds to the steering vector of a virtual array whose sensor positions can be written as

$$\mathbb{C}_d^- = \{-d_m + d_n | d_m, d_n \in \mathbb{L}\}. \tag{12}$$

Similarly, the sensor positions of virtual array corresponding to the steering vector $\mathbf{a}(\theta_k) \otimes \mathbf{a}(\theta_k)$, $\mathbf{a}^*(\theta_k) \otimes \mathbf{a}^*(\theta_k)$, and $\mathbf{a}(\theta_k) \otimes \mathbf{a}^*(\theta_k)$ are given by

$$\begin{cases} \mathbb{C}_s^+ = \{d_m + d_n | d_m, d_n \in \mathbb{L}\} \\ \mathbb{C}_s^- = \{-d_m - d_n | d_m, d_n \in \mathbb{L}\} \\ \mathbb{C}_d^+ = \{d_m - d_n | d_m, d_n \in \mathbb{L}\}, \end{cases} \tag{13}$$

respectively. Therefore, $\mathbf{B}$ can be regarded as the steering vector with the sensors located at

$$\mathbb{C} = \mathbb{C}_d^- \cup \mathbb{C}_s^+ \cup \mathbb{C}_s^- \cup \mathbb{C}_d^+. \tag{14}$$

Removing duplicated and discrete entries from $\mathbf{z}$ gives

$$\mathbf{z}_c = \mathbf{B}_c\mathbf{p} + \sigma_n^2\mathbf{e}_0, \tag{15}$$

where $\mathbf{e}_0$ is a column vector with middle element 1 and other elements 0. Then, the vectorized non-circular MUSIC algorithm [28], [30], which considers non-circular phases, can be used for DOA estimation.

Here, we present the difference and sum co-array $\mathbb{C}$, defined as

Definition 1 (difference and sum co-array). Let $\mathbb{L}$ be an integer set denoting the sensor positions. The difference and sum co-array of $\mathbb{L}$ is defined as

$$\mathbb{C} = \pm\{d_m \pm d_n | d_m, d_n \in \mathbb{L}\}. \tag{16}$$

Obviously, the difference and sum co-array is symmetric, so we often show the non-negative part only.

C. MUTUAL COUPLING

The mutual coupling between the physical sensors is not considered in equation (3). However, the mutual coupling effect between the sensors with close distance cannot be neglected in practice. We incorporate it into the received signal vector as follows,

$$\mathbf{x}(t) = \mathbf{C}\mathbf{A}\mathbf{\Phi}\bar{\mathbf{s}}(t) + \mathbf{n}(t), \tag{17}$$

where $\mathbf{C}$ represents the $Q \times Q$ mutual coupling matrix. Note that when $\mathbf{C}$ is an identity matrix, equation (17) is reduced to the coupling-free model (3).

In general, $\mathbf{C}$ is rather sophisticated. According to [14], for uniform linear arrays, $\mathbf{C}$ can be modeled by a B-banded symmetric Toeplitz matrix as

$$\langle \mathbf{C} \rangle_{d_m,d_n} = \begin{cases} c_{|d_m - d_n|}, & \text{if } |d_m - d_n| \le B \\ 0, & \text{otherwise,} \end{cases} \tag{18}$$

where $d_m, d_n \in \mathbb{L}$ and $c_0, c_1, \ldots, c_B$ are coupling coefficients satisfying $c_0 = 1 > |c_1| > |c_2| > \ldots, > |c_B|$. It is assumed that the bigger sensor separation is, the smaller magnitude of coupling coefficient is, i.e. $|c_k/c_l| = l/k$.

III. THE PROPOSED TRANSFORMED COPRIME ARRAY STRUCTURE

In this section, the shifted coprime array (SCA) is introduced by shifting one sub-array to the right by L unit spacing to yield a higher number of consecutive lags for virtual array. Then, we propose the coprime array with shifted and flipped sub-array (CASFS) with a much sparser structure than SCA, reducing the effect of mutual coupling.

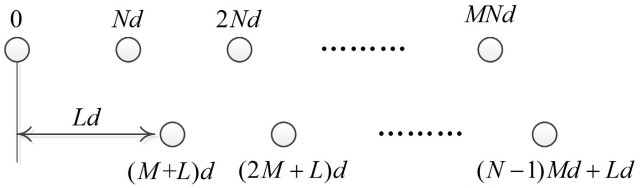

FIGURE 1. Topological structure of the shifted coprime array.

A. THE SHIFTED COPRIME ARRAY

In order to further improve the virtual array aperture, we propose a shifted coprime array by shifting one sub-array to the right and fixing another one. The novel coprime array structure provides a higher number of consecutive lags and a larger physical array aperture. As shown in Fig.1, the SCA consists of two sub-arrays with $M+1$ and $N-1$ sensors, denoted by $\mathbb{L}_1$ and $\mathbb{L}_2$, respectively, where M and N are coprime, and $\mathbb{L}_2$ is shifted Ld to the right. The sensor positions of SCA can be expressed as

$$\begin{cases} \mathbb{L} = \mathbb{L}_1 \cup \mathbb{L}_2 \\ \mathbb{L}_1 = \{mNd | m \in \mathbb{M}\} \\ \mathbb{L}_2 = \{nMd + Ld | n \in \mathbb{N}\}, \end{cases} \tag{19}$$

where $\mathbb{M} = [0, M]$ and $\mathbb{N} = [1, N-1]$. Then, according to Definition 1, the difference and sum co-array of SCA can be expressed as

$$\mathbb{C} = \pm\{\mathbb{S}_{i,j} \cup \mathbb{D}_{i,j}\}, \quad i, j \in \{1, 2\}, \tag{20}$$

where $\mathbb{S}_{i,j} = sum(\mathbb{L}_i, \mathbb{L}_j)$ and $\mathbb{D}_{i,j} = diff(\mathbb{L}_i, \mathbb{L}_j)$ represent the sum set and difference set between $\mathbb{L}_i$ and $\mathbb{L}_j$, respectively. Specifically, the sum sets of sub-arrays are given by

$$\begin{cases} \mathbb{S}_{1,1} = \{mN | 0 \le m \le 2M\} \\ \mathbb{S}_{1,2} = \{mN + nM + L | m \in \mathbb{M}, n \in \mathbb{N}\} \\ \mathbb{S}_{2,2} = \{nM + 2L | 2 \le n \le 2N - 2\}, \end{cases} \tag{21}$$

whereas the difference co-array of sub-arrays are given by

$$\begin{cases} \mathbb{D}_{1,1} = \{mN | 0 \le m \le M\} \\ \mathbb{D}_{1,2} = \{mN - nM - L | m \in \mathbb{M}, n \in \mathbb{N}\} \\ \mathbb{D}_{2,1} = \{nM + L - mN | m \in \mathbb{M}, n \in \mathbb{N}\} \\ \mathbb{D}_{2,2} = \{nM | 0 \le n \le N - 2\}. \end{cases} \tag{22}$$

Obviously, $\mathbb{D}_{1,2}$ is the mirror of $\mathbb{D}_{2,1}$, i.e. $\mathbb{D}_{1,2} = -\mathbb{D}_{2,1}$.

The following proposition summarizes the properties of $\mathbb{S}_{1,2}$ and $\mathbb{D}_{2,1}$ of SCA.

Proposition 1: Set $\mathbb{S}_{1,2}$ and set $\mathbb{D}_{2,1}$ have the following properties:

(A) The relationship between $\mathbb{S}_{1,2}$ and $\mathbb{D}_{2,1}$ can be expressed as

$$\mathbb{S}_{1,2} = \mathbb{D}_{2,1} + MN. \tag{23}$$

(B) In the range of $\mathbb{D}_{2,1}$, there exists holes located at

$$\mathbb{H}_{2,1}^{d} = \mathbb{H}_1 \cup \{L\} \cup \mathbb{H}_2, \tag{24}$$

where

$$\mathbb{H}_1 = \{aM + bN + L | a \ge 0, b > 0, \\ 0 < aM + bN < M(N-1)\}, \tag{25}$$

and

$$\mathbb{H}_2 = \{L - (cM + dN) | c \ge 0, d > 0, \\ 0 < cM + dN < M(N-1)\}. \tag{26}$$

(C) In the range of $\mathbb{S}_{1,2}$, there exists holes located at

$$\mathbb{H}_{1,2}^{s} = \mathbb{H}_3 \cup \{MN + L\} \cup \mathbb{H}_4, \tag{27}$$

where $\mathbb{H}_3 = \mathbb{H}_1 + MN$ and $\mathbb{H}_4 = \mathbb{H}_2 + MN$.

(D) Let $\mathbb{C}_1 = \mathbb{S}_{1,2} \cup \mathbb{D}_{2,1}$, then in the range of $\mathbb{C}_1$, there exists holes located at

$$\mathbb{H}_{ds} = \mathbb{H}_2 \cup \mathbb{H}_{1,4}^{r} \cup \mathbb{H}_3 \cup \{L, MN + L\}, \tag{28}$$

where

$$\mathbb{H}_{1,4}^{r} = \{\alpha N + L | L < \alpha N + L < MN + L\}. \tag{29}$$

Proof: See Appendix A.

In order to facilitate the analysis of the virtual array structure, we first exploit the virtual array generated by the $\pm\mathbb{C}_1 \cup \pm\mathbb{S}_{1,1}$. According to (21) and (28), we know that, as L changes, $\pm\mathbb{S}_{1,1}$ will not change, but the position of holes in the range of $\pm\mathbb{C}_1$ will change. To generate a virtual array with higher DOFs for SCA, we consider constructing $\pm\mathbb{C}_1$ whose holes can be as much as possible filled with $\pm\mathbb{S}_{1,1}$ by choosing a suitable value of L. Hence, we present the proposition as follow:

Propositon 2: Let $\mathbb{L}$ be a SCA with parameters M, N and L. $L = \lfloor (M+1)/2 \rfloor N$ is the optimal choice that yields the largest number of consecutive lags for SCA, and the consecutive lags are given by

$$\mathbb{C}_c = \{\phi | -\Phi + 1 \le \phi \le \Phi - 1\}, \tag{30}$$

where $\Phi = MN + M + N + L$.

Proof: See Appendix B.

In order to illustrate Proposition 1 and Proposition 2 more clearly, we set $(M, N) = (5, 4)$ generating a SCA as an example here. According to Proposition 2, we shift sub-array $\mathbb{L}_2$ to the right by $L = 12$. Fig.2 shows the result, where red squares denote the sensors of sub-array A, blue circles denote the sensors in sub-array B, black squares represent virtual elements and crosses stand for holes. The positions of physical sensors $\mathbb{L}$ can be specified as $\mathbb{L}_1 = \{0, 4, 8, 12, 16, 20\} \cup \mathbb{L}_2 = \{17, 22, 27\}$. It can be observed that the holes in the range of $\mathbb{D}_{2,1}$ are located at $\mathbb{H}_2 = \{-2, -1, 0, 3, 4, 8\} \cup \{12\} \cup \mathbb{H}_1 = \{16, 20, 21, 24, 25, 26\}$, and the holes in the range of $\mathbb{S}_{1,2}$ are located at $\mathbb{H}_4 = \{18, 19, 20, 23, 24, 28\} \cup \{32\} \cup \mathbb{H}_3 = \{36, 40, 41, 44, 45, 46\}$. Therefore, $\mathbb{S}_{1,2}$ can be regarded as a set generated by adding MN to each element of $\mathbb{D}_{2,1}$, indicating that $\mathbb{S}_{1,2}$ and $\mathbb{D}_{2,1}$ possess similar virtual array structure. By combining the ranges of $\mathbb{S}_{1,2}$ and $\mathbb{D}_{2,1}$, we can see that, in the overlapping range [17, 27], the holes of $\mathbb{H}_4$ located at $\{18, 19, 23\}$ are filled by the elements

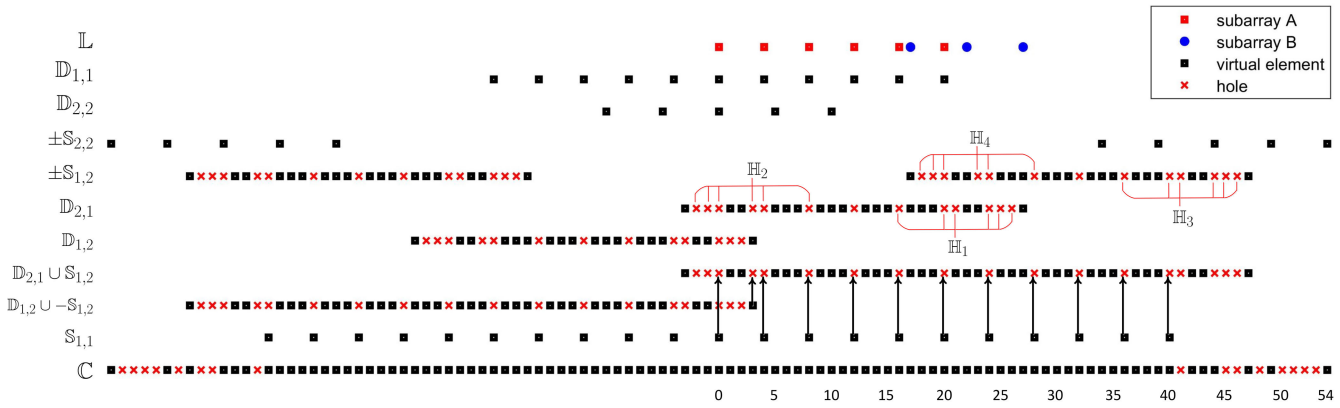

FIGURE 2. An example of SCA configuration co-array, where $M = 5, N = 4, L = 12$.

in $\mathbb{D}_{2,1}$, and the holes of $\mathbb{H}_1$ with position $\{21, 25, 26\}$ are filled with the elements in $\mathbb{S}_{1,2}$, so that the remaining holes in the overlapping range $[17, 27]$ are at $\{20, 24\}$. Therefore, the holes in the range of $\mathbb{D}_{2,1} \cup \mathbb{S}_{1,2}$ are located at $\{0, 3, 4, 8, 12, 16, 20, 24, 28, 32, 36, 40\} \cup \{41, 44, 45, 46\}$. In addition, the hole at $\{3\}$ can be filled by $\mathbb{D}_{1,2}$ and the holes at $\{0, 4, 8, 12, 16, 20, 24, 28, 32, 36, 40\}$ are integer multiples of 4, making that they can be filled by $\mathbb{S}_{1,1}$. As a result, the hole located at $\{41\}$ is the first hole that cannot be filled, so that the number of consecutive lags of the SCA is 81.

B. OPTIMAL SENSOR ALLOCATION PROBLEM

In this subsection, we will address the problem of the optimal sensor distribution to maximize the number of consecutive lags for a given number of physical sensors. According to the above Propositions, the number of consecutive lags of the SCA is $2\Phi + 1$. Hence, the optimization problem about the number of consecutive lags can be formulated as

$$\begin{aligned} &\max\ (MN + M + N + \lfloor (M+1)/2 \rfloor N) \\ &\textit{subject to}\ M + N = Q \\ &\qquad gcd(M, N) = 1 \\ &\qquad M, N \geq 2. \end{aligned} \tag{31}$$

In other words, what we are interested in is how to configure (M, N) to make virtual ULA largest under a fixed number of sensors. The solution to (31) can then be given by the following proposition.

Proposition 3: One solution to the optimization problem in (31) can be expressed as

$$M_{opt} = \begin{cases} \frac{Q}{2} - 1, & \text{if } Q \text{ is even}, \ \frac{Q}{2} \text{ is even} \\ \frac{Q}{2} - 2, & \text{if } Q \text{ is even}, \ \frac{Q}{2} \text{ is odd} \\ \frac{Q-1}{2}, & \text{if } Q \text{ is odd}, \ \frac{Q+1}{2} \text{ is even} \\ \frac{Q+1}{2}, & \text{if } Q \text{ is odd}, \ \frac{Q+1}{2} \text{ is odd}, \end{cases} \tag{32}$$

then $N_{opt} = Q - M_{opt}$.

According to (32), we can obtain M_{opt} is an odd and $L_{opt} = (M+1)/2$. The length of the corresponding consecutive lags of one-side virtual uniform linear array can be written as

$$\Phi = \begin{cases} \frac{3}{8}Q^2 + \frac{5}{4}Q - 2, & \text{if } Q \text{ is even}, \ \frac{Q}{2} \text{ is even} \\ \frac{3}{8}Q^2 + \frac{5}{4}Q - 6, & \text{if } Q \text{ is even}, \ \frac{Q}{2} \text{ is odd} \\ \frac{3}{8}Q^2 + \frac{5}{4}Q - \frac{9}{8}, & \text{if } Q \text{ is odd}, \ \frac{Q+1}{2} \text{ is even} \\ \frac{3}{8}Q^2 + \frac{5}{4}Q - \frac{13}{8}, & \text{if } Q \text{ is odd}, \ \frac{Q+1}{2} \text{ is odd}. \end{cases} \tag{33}$$

Proof: See Appendix C.

For comparison, the one-side uniform DOFs for prototype coprime array (PCA) and diff-sum improved coprime array (DSICA) are also given by

prototype coprime array [27]:

$$\Phi = \begin{cases} \frac{1}{4}Q^2 + \frac{3}{2}Q, & \text{if } Q \text{ is even} \\ \frac{1}{4}Q^2 + \frac{3}{2}Q - \frac{15}{4}, & \text{if } Q \text{ is odd}, \ \frac{Q-1}{2} \text{ is even} \\ \frac{1}{4}Q^2 + \frac{3}{2}Q - \frac{3}{4}, & \text{if } Q \text{ is odd}, \ \frac{Q-1}{2} \text{ is odd}, \end{cases} \tag{34}$$

diff-sum improved coprime array [31]:

$$\Phi = \begin{cases} \frac{1}{4}Q^2 + \frac{3}{2}Q - 1 & \text{if } Q \text{ is even}, \ \frac{Q}{2} \text{ is even} \\ \frac{1}{4}Q^2 + \frac{3}{2}Q - 3 & \text{if } Q \text{ is even}, \ \frac{Q}{2} \text{ is odd} \\ \frac{1}{4}Q^2 + \frac{3}{2}Q - \frac{3}{4} & \text{if } Q \text{ is odd}. \end{cases} \tag{35}$$

From (33), (34), and (35), it is observed that the number of consecutive lags for the SCA, PCA, and DSICA have the same order of magnitude of N^2. Moreover, the SCA possesses a greater value than the PCA and DSICA. Therefore, we can

TABLE 1. Comparison of the number of consecutive lags of six kinds of sparse arrays for different number of sensors.

Array Structures	Number of sensors														
	5	7	8	9	10	11	12	13	14	15	16	17	18	19	20
PCA	21	45	57	61	81	93	109	117	141	157	177	189	217	237	261
DsCAMpS	21	45	57	61	65	—	85	—	113	133	137	165	181	—	225
DSICA	27	45	55	67	75	93	107	123	135	157	175	195	211	237	259
TNA-I	33	61	77	97	117	141	165	193	221	253	285	321	357	397	437
TNA-II	33	65	81	101	129	153	177	205	237	269	301	377	377	417	457
SCA	29	53	65	81	89	117	135	157	171	205	229	257	277	317	347

† "—" indicates that the DsCAMpS cannot produce the corresponding configuration under this number of sensors.

draw a conclusion that the SCA provides a higher number of consecutive lags than the prototype coprime array and diff-sum improved coprime array. Table 1 exhibits the number of consecutive lags of six kinds of sparse arrays for different number of sensors. We observe that the PCA and the DSICA have almost the same number of consecutive lags, and SCA has higher DOFs than PCA, DsCAMpS, and DSICA, but lower DOFs than TNA-I and TNA-II.

C. WEIGHT FUNCTIONS

Compared with the prototype coprime array, the shifted coprime array has another advantage which is less affected by mutual coupling. From [14], we know that the inter-element spacing determines the effect of mutual coupling and the weight function with $l \in \{1, 2, 3\}$, implying sensors pair of them are separated by small inter-element spacing, has a great influence on the mutual coupling of an array. In this subsection, we derive the expression of weight function for the SCA to evaluate the effect of mutual coupling.

Proposition 4: Let $\mathbb{L}$ be an SCA with parameters M, N, L, where M is optimal, defined as (32), and then $L = (M + 1)N/2$. The weight function of $\mathbb{L}$ is given by

$$w(l) = \begin{cases} M+N, & l = 0 \\ N-j, & 1 \le j \le N-2, l = \pm jM \\ M-j, & 0 \le j \le M-1, l = \pm(j+1)N \\ 1, & l \in \pm\mathbb{D}_{1,2}, \end{cases} \tag{36}$$

Proof: See Appendix D.

According to Proposition 4, we obtain

$$w(1) = w(2) = w(3) = 1, \tag{37}$$

when $\min(M, N)$>3. Because M is odd, it must not be 2. Therefore, when $N = 2$, the weight functions for $l = 1, 2, 3$ is given by

$$w(1) = 1, w(2) = M - 1, w(3) = 1. \tag{38}$$

When $M = 3$, the weight functions for $l = 1, 2, 3$ can be expressed as

$$w(1) = 1, w(2) = 1, w(3) = N - 1. \tag{39}$$

For comparison, the first three weight functions for PCA are given by

$$w(1) = 2, w(2) = 2, w(3) = 2. \tag{40}$$

Through (37) and (40), we observe that the SCA possesses smaller values of $w(1)$, $w(2)$, $w(3)$ than the PCA.

D. THE SHIFTED AND FLIPPED COPRIME ARRAY

Although the shifted coprime array has a small value of $w(1)$, $w(2)$, and $w(3)$, it is still affected by mutual coupling greatly. In this subsection, we propose a coprime array with shifted and flipped sub-array having the weight functions $w(1) = w(2) = w(3) = 0$ and keeping the same virtual array aperture as the SCA. It can be obtained by flipping the sub-array B of the SCA with the zero point as the symmetry point. Therefore, the position sets of the CASFS are given by

$$\begin{cases} \widetilde{\mathbb{L}} = \widetilde{\mathbb{L}}_1 \cup \widetilde{\mathbb{L}}_2 \\ \widetilde{\mathbb{L}}_1 = \{mNd | m = 0, 1, \ldots, M\} \\ \widetilde{\mathbb{L}}_2 = \{-nMd - Ld | n = 1, 2, \ldots, N-1\}. \end{cases} \tag{41}$$

By analyzing the virtual array of the SCA and CASFS, their relationship can be revealed as follow:

Proposition 5: Let $\widetilde{\mathbb{L}}$ be a shifted and flipped coprime array generated by flipping the sub-array B of a shifted coprime array $\mathbb{L}$. Then the diff-sum co-array of $\mathbb{L}$ and $\widetilde{\mathbb{L}}$ denoted by $\mathbb{C}$ and $\widetilde{\mathbb{C}}$ respectively are the same, i.e.

$$\mathbb{C} = \widetilde{\mathbb{C}}. \tag{42}$$

Proof: The diff-sum co-array of the SCA can be rewritten as

$$\mathbb{C} = \pm\{\mathbb{S}_{1,1} \cup \mathbb{D}_{1,1} \cup \mathbb{S}_{2,2} \cup \mathbb{D}_{2,2} \cup \mathbb{S}_{1,2} \cup \mathbb{D}_{1,2}\}, \tag{43}$$

where

$$\begin{cases} \mathbb{D}_{1,1} = \{d_m - d_n | d_m, d_n \in \mathbb{L}_1\} \\ \mathbb{D}_{1,2} = \{d_m - d_n | d_m \in \mathbb{L}_1, d_n \in \mathbb{L}_2\} \\ \mathbb{D}_{2,2} = \{d_m - d_n | d_m, d_n \in \mathbb{L}_2\} \\ \mathbb{S}_{1,1} = \{d_m + d_n | d_m, d_n \in \mathbb{L}_1\} \\ \mathbb{S}_{1,2} = \{d_m + d_n | d_m \in \mathbb{L}_1, d_n \in \mathbb{L}_2\} \\ \mathbb{S}_{2,2} = \{d_m + d_n | d_m, d_n \in \mathbb{L}_2\}. \end{cases} \tag{44}$$

The diff-sum co-array of the CASFS can be expressed as

$$\widetilde{\mathbb{C}} = \pm\{\widetilde{\mathbb{S}}_{1,1} \cup \widetilde{\mathbb{D}}_{1,1} \cup \widetilde{\mathbb{S}}_{2,2} \cup \widetilde{\mathbb{D}}_{2,2} \cup \widetilde{\mathbb{S}}_{1,2} \cup \widetilde{\mathbb{D}}_{1,2}\}. \tag{45}$$

According to (19) and (41), we know $\mathbb{L}_1 = \widetilde{\mathbb{L}}_1$ and $\mathbb{L}_2 = -\widetilde{\mathbb{L}}_2$. Therefore, the relationships between the subsets of $\mathbb{C}$

TABLE 2. Simulation conditions for the experiments.

Simulation parameters	Value
Sensor positions of PCA	0,5,6,10,12,15,18,20,24,25,30
Sensor positions of DsCAMpS	0,3,4,6,8,9,12,15,16,18,20,21
Sensor positions of DSICA	-27,-21,-15,-9,0,3,8,13,18,23,28
Sensor positions of TNA-I	0,6,12,18,24,30,31,32,33,34,35
Sensor positions of TNA-II	0,6,12,18,24,30,33,34,35,37,38
Sensor positions of CASFS	-43,-38,-33,-28,-23,0,6,12,18,24,30
Carrier frequency	$f = 2.1GHz$
Speed of light	$c = 3 \times 10^8 m/s$
Monte Carlo times	200
Signal-to-noise ratio(SNR)	$SNR = -6 \sim 20dB$

and that of $\widetilde{\mathbb{C}}$ can be expressed as

$$\begin{cases} \widetilde{\mathbb{D}}_{1,1} = \mathbb{D}_{1,1} \\ \widetilde{\mathbb{D}}_{1,2} = \pm\{d_m - d_n | d_m \in \widetilde{\mathbb{L}}_1, d_n \in \widetilde{\mathbb{L}}_2\} = \mathbb{S}_{1,2} \\ \widetilde{\mathbb{D}}_{2,2} = \pm\{d_m - d_n | d_m, d_n \in \widetilde{\mathbb{L}}_2\} = -\mathbb{D}_{2,2} \\ \widetilde{\mathbb{S}}_{1,1} = \mathbb{S}_{1,1} \\ \widetilde{\mathbb{S}}_{1,2} = \pm\{d_m + d_n | d_m \in \widetilde{\mathbb{L}}_1, d_n \in \widetilde{\mathbb{L}}_2\} = \mathbb{D}_{1,2} \\ \widetilde{\mathbb{S}}_{2,2} = \pm\{d_m + d_n | d_m, d_n \in \widetilde{\mathbb{L}}_2\} = -\mathbb{S}_{2,2}, \end{cases} \tag{46}$$

so we can obtain $\mathbb{C} = \widetilde{\mathbb{C}}$. ■

Next, we investigate the weight function of CASFS, which can be expressed as

$$\widetilde{w}(l) = \begin{cases} M+N, & l = 0 \\ N-j, & 1 \le j \le N-2, l = \pm jM \\ M-j, & 0 \le j \le M-1, l = \pm(j+1)N \\ 1, & l \in \pm\widetilde{\mathbb{D}}_{1,2}, \end{cases} \tag{47}$$

Based on (47), we conclude that the weight function of SCA and CASFS have the same value when l is an integer multiple of m, n, due to $\pm\mathbb{D}_{1,1} = \pm\widetilde{\mathbb{D}}_{1,1}$ and $\pm\mathbb{D}_{2,2} = \mp\widetilde{\mathbb{D}}_{2,2}$.

Remark: $\widetilde{\mathbb{D}}_{1,2}$ is not equal to $\mathbb{D}_{1,2}$, but equal to the cross sum set $\mathbb{S}_{1,2}$, indicating that the inter-element spacings of CASFS are increased.

Moreover, when $\min(M, N)$>3, there is no $1, 2, 3$ in $\widetilde{\mathbb{D}}$ because the minimum of inter-element spacing is $\min(M, N, \lfloor (M+1)/2 \rfloor N)$, i.e.

$$\widetilde{w}(1) = \widetilde{w}(2) = \widetilde{w}(3) = 0. \tag{48}$$

When $N = 2$, the weight functions for $l = 1, 2, 3$ are given by

$$\widetilde{w}(1) = 0, \widetilde{w}(2) = M - 1, \widetilde{w}(3) = 0, \tag{49}$$

and when $M = 3$, the weight functions for $l = 1, 2, 3$ can be expressed as

$$\widetilde{w}(1) = 0, \widetilde{w}(2) = 0, \widetilde{w}(3) = 1. \tag{50}$$

From (37) and (48), we observe that the CASFS is less affected by mutual coupling than SCA and PCA.

IV. SIMULATION RESULTS

In this section, simulation results are presented to illustrate the advantages of the proposed array structure. In all DOA estimations, we suppose that the number of sources is known and that all incident signals have equal power. The NC phases of signals are randomly distributed between 0 and π. To evaluate the performance quantitatively, we define the root mean square error (RMSE) as

$$RMSE = \sqrt{\frac{1}{200K} \sum_{m=1}^{200} \sum_{k=1}^{K} \left(\hat{\theta}_k(m) - \theta_k\right)^2}, \tag{51}$$

where K is the number of sources, and $\hat{\theta}_k(m)$ is the k-th source DOA in the m-th Monte Carlo simulation. The simulation conditions are listed in Table 2. We set $Q = 11$ for all arrays, except for DsCAMpS which is 12, because DsCAMpS configuration does not exist for $Q = 11$.

A. WEIGHT FUNCTION AND MUTUAL COUPLING MATRICES

The first set of simulations compares the weight functions and mutual coupling matrices of PCA [10], DsCAMpS [28], DISCA [31], TNA-I [30], TNA-II [30], and CASFS. For all these arrays, their structure configurations are listed in the Table 2. Here, we consider the scenario with heavy mutual coupling, where the coupling parameters are given by $c_1 = 0.3e^{j\pi/3}$, $B = 100$, and $c_l = c_1 e^{-j(l-1)\pi/8}/l$ for $2 \le l \le B$. Fig.3 presents the weight functions for the six kinds of sparse linear arrays (SLAs). As shown in Fig.3, TNA-I has the highest weight functions with $w(1) = 5, w(2) = 4, w(3) = 3$, while $w(1) = w(2) = w(3) = 2$ for the PCA, $w(1) = 3, w(2) = 2, w(3) = 2$ for the TNA-II, $w(1) = 4, w(2) = 4, w(3) = 7$ for the DsCAMpS. The DSICA possesses smaller weight functions with $w(1) = 0, w(2) = 0, w(3) = 1$ due to its sparser configuration. The CASFS provides excellent set of weight functions among all the arrays with $w(1) = w(2) = w(3) = 0$. Fig. 4 exhibits the magnitudes of the mutual coupling matrices for the six kinds of SLAs. The blue color implies less energy in the corresponding entry. According to [14], the mutual coupling leakage is defined as

$$L = \frac{||\mathbf{C} - diag(\mathbf{C})||_F}{||\mathbf{C}||_F} \tag{52}$$

TABLE 3. A summary of mutual coupling leakage for six kinds of sparse linear arrays.

Array	TNA-I	DsCAMpS	TNA-II	PCA	DSICA	CASFS
L	0.3163	0.3026	0.2590	0.2304	0.0947	0.0805

A small value of L indicates that a mutual coupling is weak. Table 3 lists a summary of L for the six different sparse linear arrays. It can be observed that TNA-I and DsCAMpS yield higher values of mutual coupling leakage with L>0.3 than the other arrays, indicating that they suffer

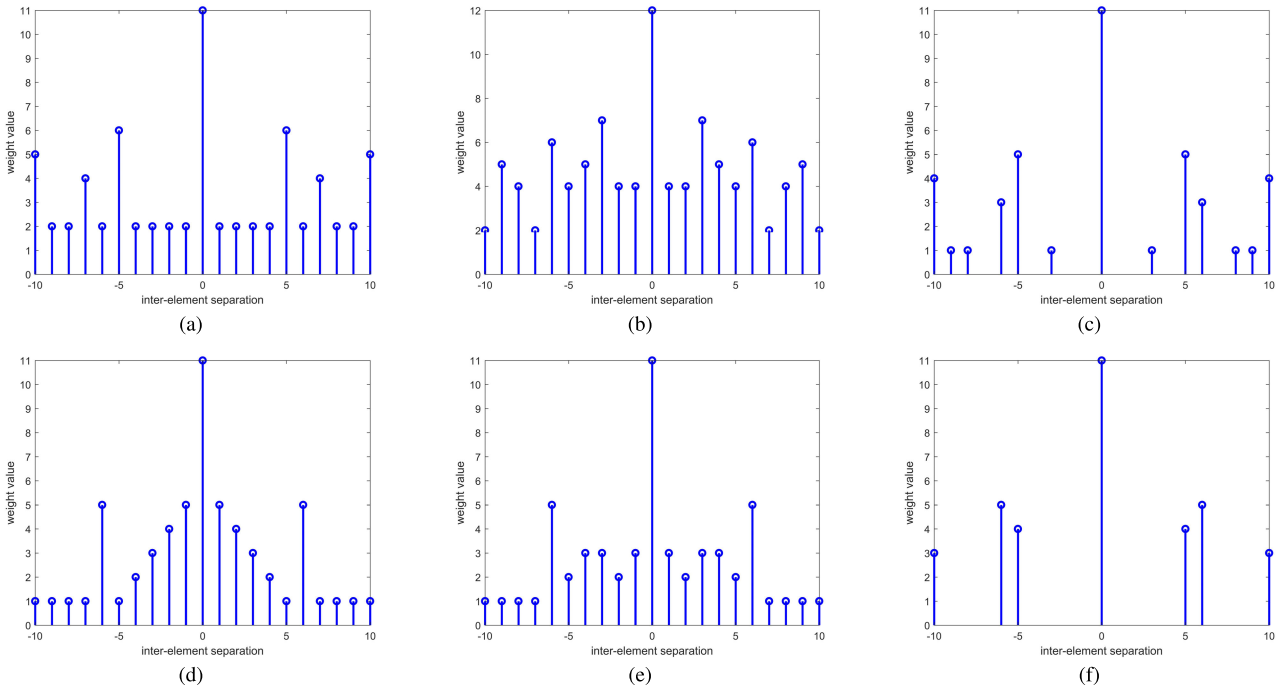

FIGURE 3. The weight functions for six kinds of SLAs. (a) PCA. (b) DsCAMpS. (c) DSICA. (d) TNA-I. (e) TNA-II. (f) CASFS.

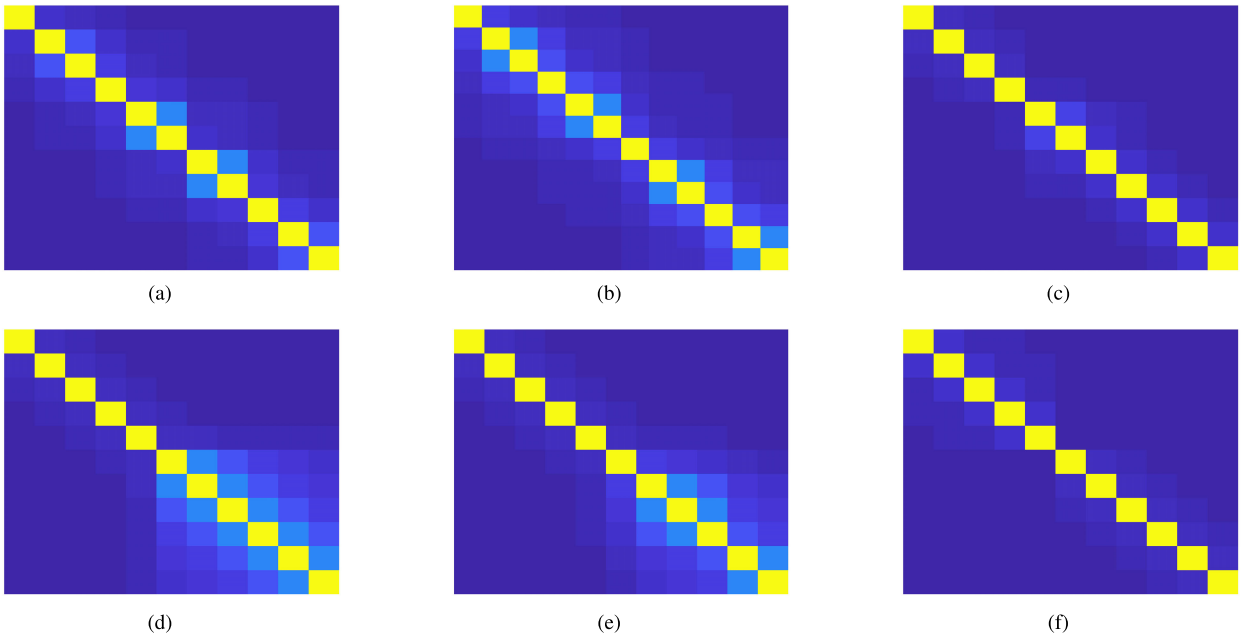

FIGURE 4. The magnitudes of the mutual coupling matrices for six kinds of SLAs. (a) PCA. (b) DsCAMpS. (c) DSICA. (d) TNA-I. (e) TNA-II. (f) CASFS.

from serious mutual coupling effect, while the PCA and TNA-II can moderately reduce the mutual coupling effect and the DSICA is much less sensitive to the mutual coupling effect. The CASFS offers the least value of L, implying the weakest mutual coupling effect among all the six kinds of SLAs.

B. DOA ESTIMATION IN THE PRESENCE OF MUTUAL COUPLING

In the second set of simulations, we present the MUSIC spectra of the six kinds of SLAs to compare the capability of distinguishing sources in presence of heavy mutual coupling, and then simulate the RMSE of these arrays against SNR,

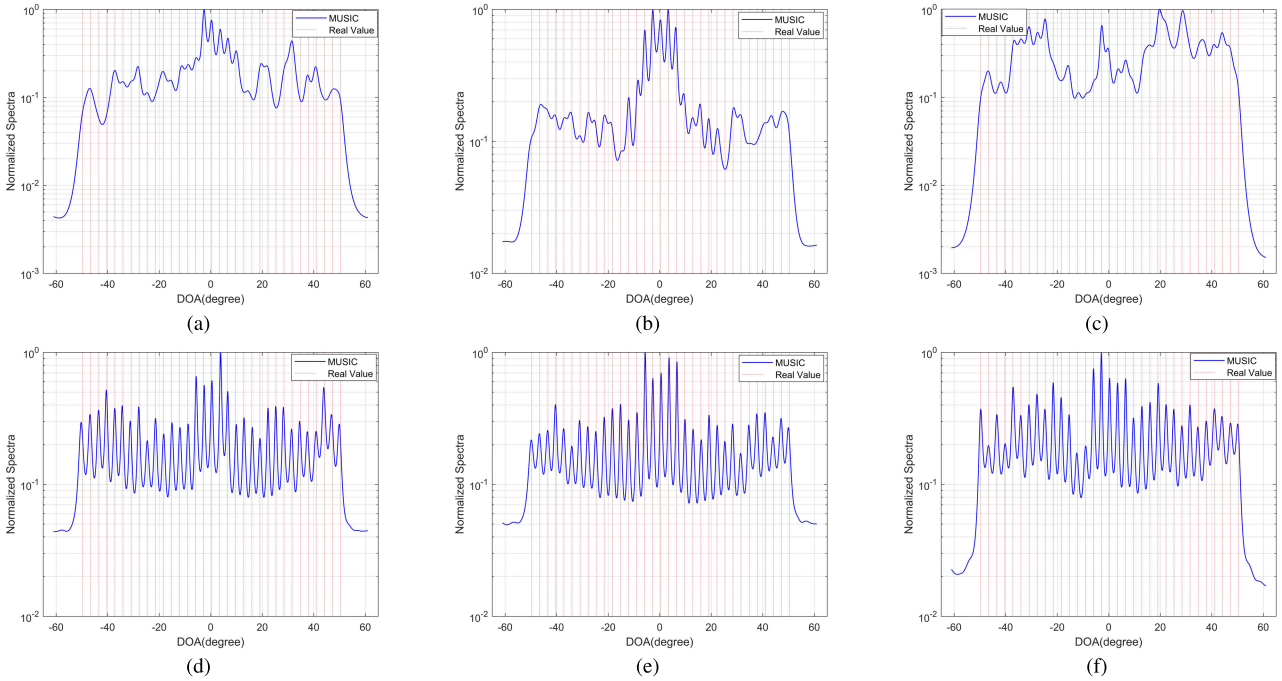

FIGURE 5. The MUSIC spectra for six kinds of SLAs when $K = 33$ sources are located at $\theta_k = -50° + 100°(k-1)/32$, $1 \le k \le 33$. (a) PCA. (b) DsCAMpS. (c) DSICA. (d) TNA-I. (e) TNA-II. (f) CASFS.

the number of snapshots, the number of sources, and mutual coupling intensity.

1) MUSIC Spectra: In this simulation, the SNR is fixed at 10dB and the number of frames and snapshots is $F = 50$ and $T = 500$, while $c_1 = 0.3e^{j\pi/3}$. Fig.6 depicts the MUSIC Spectra for six kinds of SLAs when $K = 33$ sources are located at $\theta_k = -50° + 100°(k-1)/32$, $1 \le k \le 33$. From Fig.5, it can be seen that the TNA-I, TNA-II and CASFS are capable of distinguishing all 33 sources, while the PCA, DsCAMpS and DSICA can hardly work. This is because TNA-I and TNA-II have a large number of consecutive lags, while CASFS has a weaker mutual coupling effect, although its consecutive lags number is not as large as TNA. Therefore, we can conclude that the CASFS and TNA outperform the remaining arrays under heavy mutual coupling and underdetermined conditions.

2) RMSE Performance: The next simulations focus on the RMSE performance with respect to the input SNR, the number of snapshots, the number of sources, and the modulus of coupling coefficient c_1. The mutual coupling model is characterized by $B = 100$, $c_1 = 0.3e^{j\pi/3}$ and $c_l = c_1 e^{-j(l-1)\pi/8}/l$ (except the case where c_1 varies). The fixed parameter settings are SNR $= 10$dB, $T = 500$ snapshots, $F = 50$ frames and $K = 15$ sources (except the case where K varies). The sources are located at $\theta_k = -50° + 100°(k-1)/14$, $1 \le k \le 15$.

Fig. 6 shows the RMSE of the DOA estimates as a function of the input SNR. We can observe that the RMSEs of the TNA-I, TNA-II and DsCAMpS do not change much with the increase of the SNR, because their dense sub-array structures

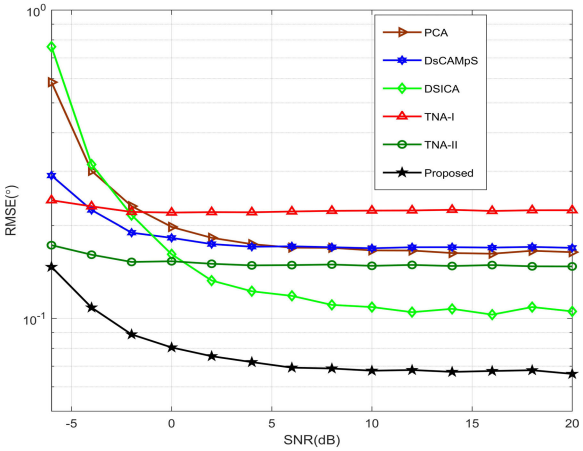

FIGURE 6. RMSE versus the input SNR, where $K = 15$, $F = 50$, and $T = 500$.

make them severely affected by mutual coupling. On the contrary, the RMSEs of the other three SLAs decrease as the SNR increases and reach a stable level until the SNR is higher than 10dB, while the CASFS possesses the lowest RMSE over the entire SNR ranges among all these arrays. It implies that the proposed array outperforms the other arrays against mutual coupling effects due to its sparser structure.

The RMSE of the DOA estimates with respect to the number of snapshots is presented in Fig. 7. We observe that, along with the number of snapshots increase, the RMSE is reduced rapidly for the CASFS and DSICA until T reaches about 400, and the CASFS exhibits the lowest RMSE among

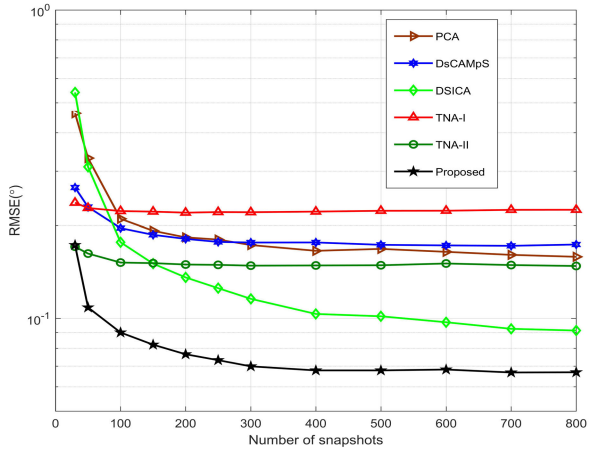

FIGURE 7. RMSE versus the number of snapshots, where $K = 15$, SNR = 10dB, and $F = 50$.

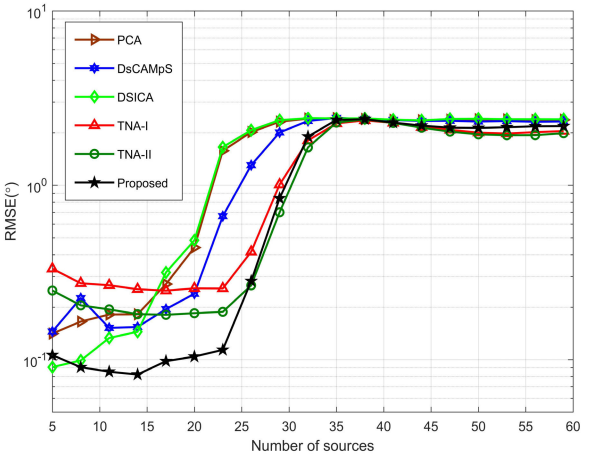

FIGURE 10. RMSE versus the number of sources, where SNR = 10dB, $F = 50$, and $T = 500$.

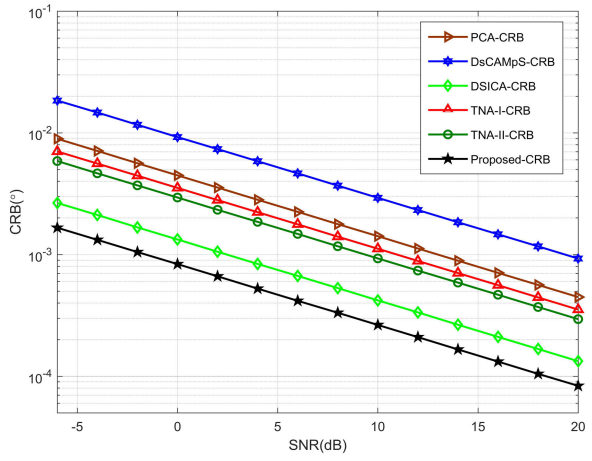

FIGURE 8. CRB versus the input SNR, where $F = 50$, $T = 500$.

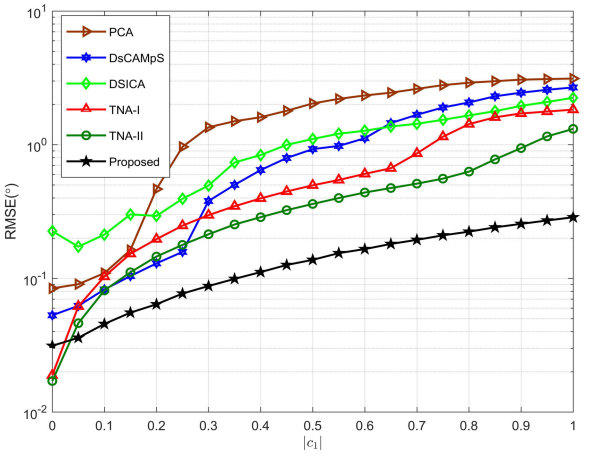

FIGURE 11. RMSE versus varying modulus of mutual coupling, where $K = 22$, SNR = 10dB, $F = 50$, and $T = 500$.

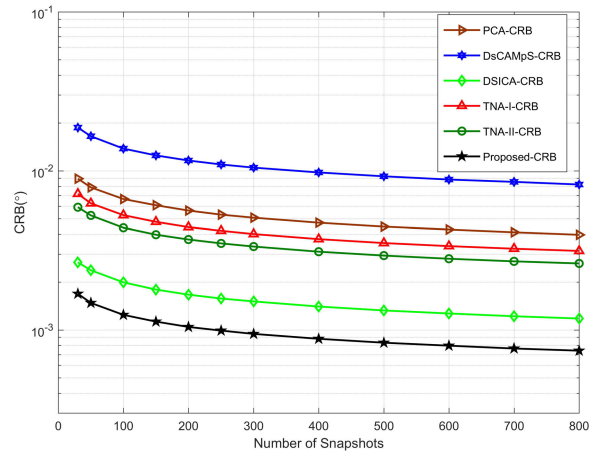

FIGURE 9. CRB versus the number of snapshots, where SNR = 10dB, $F = 50$.

all these arrays. In contrast, the RMSEs of other arrays are reduced rather slowly, especially for the TNA-I and TNA-II. The Cramer-Rao lower bound (CRB) is the lower bound of the unbiased estimation variance, which is used to measure the deviation of the DOA estimation. Based on [4] and [33], we simulate the CRB of the six kinds of sparse array. Fig. 8 and Fig. 9 show the results of the CRB of the DOA estimation of the different sparse arrays. We see that the CRB of CASFS is lower than that of the other arrays, and the accuracy of DOA estimation is improved obviously.

The RMSE of the DOA estimates versus the number of sources is illustrated in Fig. 10. When $K > 23$, the RMSEs of these six kinds of array suffer from rapid deterioration because of severe mutual coupling. The CASFS performs best than the remaining arrays for the number of sources is less than 23. The RMSE of the DOA estimates with varying $|c_1|$ is plotted in Fig. 11. It can be seen that as the increase of $|c_1|$, the corresponding RMSE for all these arrays increases. That is because a higher value of $|c_1|$ introduces a higher level mutual coupling effect. When $c_1 = 0$, the TNA-I and TNA-II have lower RMSE than due to higher numbers of consecutive lags than the other arrays. In the range of $|c_1| \geq 0.05$, the RMSE of CASFS is lowest among all these arrays,

indicating that the CASFS outperforms other arrays across a wide range of mutual coupling coefficients.

V. CONCLUSION

In this paper, a new coprime array structure, termed as coprime array with shifted and flipped sub-array, is proposed which provides a higher number of consecutive lags than the PCA with the same number of sensors by shifting the sub-array. Moreover, it is able to tolerate severe mutual coupling because of the sparser structure generated by flipping the shifted sub-array with the zero point as the symmetry point. For CASFS, the closed-form expression of the number of consecutive lags is derived and the optimal distribution of two sub-arrays is offered for a given number of sensors. The theoretical analysis of weight function shows that CASFS is less sensitive to mutual coupling effects compared to PCA, DsCAMps, DSICA, TNA-I, and TNA-II. Numerical simulations verify that the proposed array has a stable and decent performance of DOA estimation in presence of mutual coupling.

APPENDIX A
PROOF OF PROPOSITION 1

A. PROOF OF PROPERTY A

According to (22), an arbitrary element in $\mathbb{D}_{2,1}$ can be expressed as

$$d_{2,1} = n_1 M - m_1 N + L, \tag{53}$$

where $1 \le n_1 \le N-1$ and $0 \le m_1 \le M$. Adding MN to $d_{2,1}$ gives

$$d_{2,1} + MN = n_2 M + m_2 N + L, \tag{54}$$

where $n_1 = n_2$ and $m_2 = M - m_1$. Since $1 \le n_2 \le N-1$ and $0 \le m_2 \le M$, we obtain $\{d_{2,1} + MN\} \in \mathbb{S}_{1,2}$. Similarly, we can prove $\{s_{1,2} - MN\} \in \mathbb{D}_{2,1}$, where $s_{1,2}$ denotes an arbitrary element of $\mathbb{S}_{1,2}$. ■

B. PROOF OF PROPERTY B

Here, contradiction is used to show that the elements in $\mathbb{H}_1$ denoted by h_1 must not belong to $\mathbb{D}_{2,1}$. Supposing $h_1 \in \mathbb{D}_{2,1}$, then the equation

$$aM + bN + L = nM + L - mN \tag{55}$$

holds, where a, b, n and m satisfy $a \ge 0$, $b>0$, $1 \le n \le N-1$ and $0 \le m \le M$, respectively. Further, (55) can be rewritten as

$$\frac{M}{N} = \frac{m+b}{n-a}. \tag{56}$$

Since $n-a < N$ and the coprimality of M and N, we cannot find an integer m that satisfies (56). Therefore, hypothesis $h_1 \in \mathbb{D}_{2,1}$ doesn't hold, i.e. there are holes at $\mathbb{H}_1$ is the range of $\mathbb{D}_{2,1}$. The processes of proving holes at $\mathbb{H}_2$ and $\{L\}$ is similar to $\mathbb{H}_1$. ■

C. PROOF OF PROPERTY C

According to property (B), we can obtain $h_1 \notin \mathbb{D}_{2,1}$, then $\{h_1+MN\} \notin \mathbb{D}_{2,1}+MN$. Since $\mathbb{S}_{1,2} = \mathbb{D}_{2,1}+MN$, we obtain $\{h_1+MN\} \notin \mathbb{S}_{1,2}$. Therefore, $\mathbb{S}_{1,2}$ can be seen as the set $\mathbb{D}_{2,1}$ adding MN, and the holes in the range of $\mathbb{S}_{1,2}$ can be given by adding MN to $\mathbb{H}_1$, $\mathbb{H}_2$ and $\{L\}$. ■

D. PROOF OF PROPERTY D

Based on (21) and (22), we can obtain

$$\begin{cases} M + L \le s_{1,2} \le MN + M(N-1) + L \\ L - M(N-1) \le d_{2,1} \le M(N-1) + L, \end{cases} \tag{57}$$

where $s_{1,2} \in \mathbb{S}_{1,2}$ and $d_{2,1} \in \mathbb{D}_{2,1}$. Hence, there exists an overlapping range between $\mathbb{S}_{1,2}$ and $\mathbb{D}_{2,1}$, given by

$$\mathbb{O}_1 = \{o_1 | M + L \le o_1 \le M(N-1) + L\}. \tag{58}$$

In the overlapping range, some holes in $\mathbb{H}^d_{2,1}$ may be filled by elements of $\mathbb{S}_{1,2}$, and some holes in $\mathbb{H}^s_{1,2}$ may be filled by elements of $\mathbb{D}_{2,1}$. Hence, we further exploit which holes are filled and which are still retained in the range of $\mathbb{S}_{1,2} \cup \mathbb{D}_{2,1}$. According to properties (B) and (C), we have

$$\begin{cases} L < h_1 < L + M(N-1) \\ L - M(N-1) < h_2 < L \\ L + MN < h_3 < L + 2\text{MN-M} \\ L + M < h_4 < L + MN, \end{cases} \tag{59}$$

where $h_1 \in \mathbb{H}_1$, $h_2 \in \mathbb{H}_2$, $h_3 \in \mathbb{H}_3$ and $h_4 \in \mathbb{H}_4$. Comparing the range of holes to the overlapping range $\mathbb{O}_1$ yields

$$\begin{cases} \mathbb{O}_1 \cap \mathbb{H}_1 \ne \varnothing \\ \mathbb{O}_1 \cap \mathbb{H}_2 = \varnothing \\ \mathbb{O}_1 \cap \mathbb{H}_3 = \varnothing \\ \mathbb{O}_1 \cap \mathbb{H}_4 \ne \varnothing \\ \mathbb{O}_1 \cap \{L, MN + L\} = \varnothing, \end{cases} \tag{60}$$

indicating that some holes in $\mathbb{H}_1$ may be filled by $\mathbb{S}_{1,2}$ and some holes in $\mathbb{H}_4$ may be filled by $\mathbb{D}_{2,1}$. Assuming that some holes in $\mathbb{H}_1$ can filled by $\mathbb{S}_{1,2}$, then the equation

$$aM + bN + L = nM + mN + L, \tag{61}$$

holds. Let's discuss equation (61) in two cases where $a > 0$ and $a = 0$.

When $a > 0$, according to (25), we can obtain $M+N+L < h_1 < M(N-1) + L$, indicating that all of them located at overlapping range $\mathbb{O}_1$. If $a \ne n$, rewriting (61) gives

$$\frac{m-b}{a-n} = \frac{M}{N}, \tag{62}$$

which cannot be established due to $m - b < M$ and the coprimality between M and N. Similarly, if $b \ne m$, (61) can not be established either. We can conclude that, for the equation (61) to be true, both $a = n$ and $b = m$ must holds. Therefore, the holes in $\mathbb{H}_1$ with $a > 0$ can be completely filled by $\mathbb{S}_{1,2}$.

When $a = 0$, (61) can be rewritten as

$$\begin{aligned} bN &= nM + mN \\ \Rightarrow \frac{b-m}{n} &= \frac{M}{N}, \end{aligned} \tag{63}$$

which cannot be established due to $n < N$ and the coprimality between M and N, indicating that none of the holes in $\mathbb{H}_1$ with $a = 0$ can be all filled by $\mathbb{S}_{1,2}$.

Hence, after being filled by $\mathbb{S}_{1,2}$, $\mathbb{H}_1$ is reduced to

$$\mathbb{H}_1^r = \{\alpha N + L | L < \alpha N + L < M(N-1)\}. \tag{64}$$

Similarly, after being filled by $\mathbb{D}_{2,1}$, the remaining holes in $\mathbb{H}_4$ is reduced to

$$\mathbb{H}_4^r = \{\alpha N + L | L + M < \alpha N + L < MN + L\}. \tag{65}$$

Combining (64) and (65) yields

$$\mathbb{H}_1^r \cup \mathbb{H}_4^r = \{\alpha N + L | L < \alpha N + L < MN + L\}. \tag{66}$$

Since the intersection of $\mathbb{O}_1$ and the range of $\mathbb{H}_2 \cup \mathbb{H}_3 \cup \{L, MN + L\}$ is empty, the holes at $\mathbb{H}_2 \cup \mathbb{H}_3 \cup \{L, MN + L\}$ haven't changed anything. ■

APPENDIX B
PROOF OF PROPOSITION 2

In the following proof, we will discuss the influence of L on $\mathbb{H}_{ds}$ and derive the optimal value of L for generating more consecutive lags. Consider a positive integer L. According to whether L can be divisible by N, it can be divided into two cases, i.e. $L = gN$ and $L = gN + u$, where g is a positive integer and $1 \le u \le N - 1$. We will discuss the two cases.

Case 1: Let $L = gN$. According to whether c is equal to zero, $\mathbb{H}_2$ can be divided into two parts

$$\mathbb{H}_2 = \mathbb{H}_2^1 \cup \mathbb{H}_2^2, \tag{67}$$

where

$$\begin{aligned} \mathbb{H}_2^1 = \{L - (cM + dN) | c > 0, d > 0, \\ 0 < cM + dN < M(N-1)\}, \end{aligned} \tag{68}$$

and

$$\mathbb{H}_2^2 = \{\bar{d}N | -M(N-1) + L < \bar{d}N < L\}, \tag{69}$$

where $\bar{d} = g - d$ and $d > 0$. Then, the union of $\mathbb{H}_{1,4}^r$, $\mathbb{H}_2^2$ and $\{L, MN + L\}$ can be expressed as

$$\mathbb{H}_g = \{\alpha N | -M(N-1) + L < \alpha N \le MN + L\}. \tag{70}$$

Therefore, the holes in the range of $\mathbb{C}_1$ can be rewritten as

$$\mathbb{H}_{ds} = \mathbb{H}_2^1 \cup \mathbb{H}_3 \cup \mathbb{H}_g. \tag{71}$$

Next, we investigate $\mathbb{H}_g$, $\mathbb{H}_2^1$ and $\mathbb{H}_3$ separately.

Firstly, we focus on $\mathbb{H}_g$. Since $\pm\mathbb{S}_{1,1} = \{mN | -2M \le m \le 2M\}$, we can conclude that all holes in $\mathbb{H}_g$ can be filled by $\pm\mathbb{S}_{1,1}$ when g satisfies

$$0 < g \le M. \tag{72}$$

Secondly, we investigate the relationship between $\mathbb{H}_2^1$ and $\mathbb{D}_{1,2}$. According to (22), the overlapping range between $\mathbb{D}_{1,2}$ and its mirror $\mathbb{D}_{2,1}$ can be expressed as

$$\mathbb{O}_2 = \{o_2 | L - M(N-1) \le o_2 \le M(N-1) - L\}, \tag{73}$$

indicating that the holes at the range of $\mathbb{D}_{2,1}$ may be filled by $\mathbb{D}_{1,2}$. By comparing (68) to (73), we can obtain $\mathbb{O}_2 \cap \mathbb{H}_2^1 \neq \varnothing$. Therefore, we suppose that some holes in $\mathbb{H}_2^1$ can be filled by $\mathbb{D}_{1,2}$, then the equation

$$-cM - dN + L = -nM - L + mN, \tag{74}$$

holds. Since $c > 0$ and $d > 0$, according to (68), we can obtain $-M(N-1) + L < h_2^1 \le L - M - N$, where $h_2^1 \in \mathbb{H}_2^1$. If h_2^1 at overlapping range $\mathbb{O}_2$ and $c \neq n$, substituting $L = gN$ to (74) gives

$$\frac{d + m - 2g}{n - c} = \frac{M}{N}, \tag{75}$$

which cannot be established due to $n - c < N$ and the coprimality between M and N. Similarly, if $d + M \neq 2g$, (74) can not be established. It can be concluded that, for the equation (74) to be true, both $n = c$ and $m = 2g - d$ must holds. Therefore, the holes in $\mathbb{H}_2^1$ can be all filled by $\mathbb{D}_{1,2}$. However, as the increase of L, some holes of $\mathbb{H}_2^1$ may exceed the overlapping range $\mathbb{O}_2$ such that it can not be filled by $\mathbb{D}_{1,2}$. To ensure all holes in $\mathbb{H}_2^1$ can be filled, we need to make

$$L - M - N \le M(N-1) - L \tag{76}$$

be true. Since $L = gN$ and g is a positive integer, we obtain

$$0 < g \le \left\lfloor \frac{M+1}{2} \right\rfloor \tag{77}$$

Finally, we focus on $\mathbb{H}_3$. When $a = 0$ and $b = 1$, we calculate that the minimum value of $\mathbb{H}_3$ denoted by h_3^1 is $MN + gN + N$. To make sure the hole h_3^1 can be filled by $\mathbb{S}_{1,1}$, we need to make $MN + gN + N \le 2MN$ be true such that

$$0 < g \le M - 1. \tag{78}$$

When $a = 1, b = 1$, the next hole of $\mathbb{H}_3$ is given by

$$h_3^2 = MN + M + N + gN. \tag{79}$$

We will prove that this hole cannot be filled by $\mathbb{S}_{1,1}$. If h_3^2 can be filled by $\mathbb{S}_{1,1}$, there exists an integer n making

$$\begin{aligned} M + N + MN + gN &= 2mN \\ \Rightarrow 2m - M - 1 - g &= \frac{M}{N} \end{aligned} \tag{80}$$

work. As M, N are coprime, we cannot find integer m that satisfies (80). Hence, the hole h_3^2 cannot be filled by $\mathbb{S}_{1,1}$.

In addition, by comparing h_3^2 with the max value of $\mathbb{D}_{2,2}$, we get

$$\max(\mathbb{D}_{2,2}) = (N-2)M < h_3^2 \tag{81}$$

Therefore, the hole h_3^2 cannot be filled by $\mathbb{D}_{2,2}$. Next, we prove that the hole h_3^2 can be filled with $\mathbb{S}_{2,2}$ only

when $g = 1$. If it can be filled with $\mathbb{S}_{2,2} = \{nM + 2L | 2 \leq n \leq 2N - 2\}$, there exists an integer n making

$$M + N + MN + gN = nM + 2gN \tag{82}$$

work, then we can obtain

$$\frac{M + 1 - g}{1 + n} = \frac{M}{N}. \tag{83}$$

As M, N are coprime $0 \leq n \leq N - 1$, the condition that the equation (82) is $g = 1$. When $g > 1$, the hole h_3^2 cannot be filled with $\mathbb{S}_{2,2}$.

Since M and N are coprime, we obtain $M \leq 2$. Hence, we have

$$\left\lfloor \frac{M + 1}{2} \right\rfloor \leq M - 1. \tag{84}$$

Therefore, according to (72), (77), (78) and (84), setting $0 < g \leq \lfloor \frac{M+1}{2} \rfloor$ can ensure that all holes of $\mathbb{H}_g$ and $\mathbb{H}_2^1$ and the first hole of $\mathbb{H}_3$ can be filled, i.e. the holes less than $MN + M + N + L$ in the range of $\mathbb{H}_{ds}$ are all filled, where $\mathbb{H}_g \cup h_3^1$ and $\mathbb{H}_2^1$ are filled by $\mathbb{S}_{1,1}$ and $\mathbb{D}_{1,2}$, respectively. Therefore, we can conclude that, in the nonnegative range of $\pm\mathbb{C}_1 \cup \pm\mathbb{S}_{1,1}$, the first hole is located at $MN + gN + M + N$ such that the number of consecutive lags for $\pm\mathbb{C}_1 \cup \pm\mathbb{S}_{1,1}$ can be expressed as $2(MN + gN + M + N) - 1$, which indicates that the larger value of g, the higher DOFs. Hence, to generate a larger physical aperture and a higher DOFs for SCA, we choose

$$g = \left\lfloor \frac{M + 1}{2} \right\rfloor, \tag{85}$$

so that $L = \lfloor \frac{M+1}{2} \rfloor N$ is the optimal displacement of two sub-arrays.

Case 2: Let $L = gN + u$, $g > 0$ and $1 \leq u \leq N - 1$. We will prove that there is at least one hole located at $MN + L$ or $(M + 1)N + L$ in the difference and sum co-array of SCA, i.e. the number of consecutive lags of SCA is less than $2(MN + gN + M + N) - 1$.

Suppose that the hole $MN + L$ can be filled by the elements of $\mathbb{S}_{1,1}$, then the equation

$$\begin{aligned} mN &= MN + L \\ &\Rightarrow m - M - g = \frac{u}{N} \end{aligned} \tag{86}$$

holds. Because $\frac{u}{N}$ must not be an integer, the equation (86) cannot be established. Moveover, comparing the min values of $\mathbb{D}_{2,2}$, and $\mathbb{D}_{1,2}$ to $MN + L$ gives

$$\begin{cases} MN + L - \max(\mathbb{D}_{2,2}) = 2M + L > 0 \\ MN + L - \max(\mathbb{D}_{1,2}) = M + 2L > 0. \end{cases} \tag{87}$$

Therefore, the hole $MN + L$ cannot be filled by the elements of $\mathbb{S}_{1,1} \cup \mathbb{D}_{2,2} \cup \mathbb{D}_{1,2}$. Further, we prove that the elements in $\mathbb{S}_{2,2}$ cannot fill the holes $MN + L$ and $(M + 1)N + L$ at the same time. If the two holes can be filled with that, we obtain

$$\begin{aligned} n_1 M + 2gN + 2u &= MN + L \\ n_2 M + 2gN + 2u &= (M + 1)N + L \\ &\Rightarrow n_2 - n_1 = \frac{N}{M}. \end{aligned} \tag{88}$$

Because the coprimality of M and N, the equation (88) doesn't hold.

By combining the aforementioned **Case 1** and **Case 2** and by analogy, we can draw a conclusion that $L = \lfloor \frac{M+1}{2} \rfloor$ is the optimal choice that generates the largest number of consecutive lags achieving $2(MN + \lfloor \frac{M+1}{2} \rfloor + M + N) - 1$. ■

APPENDIX C
PROOF OF PROPOSITION 3

Lemma 1: Given the odd number of sensor $Q = M + N$, when M is odd and N is even, Φ defined as (30) is calculated and denoted by Φ_1. After swapping M and N, Φ is calculated and denoted by Φ_2. Then,

$$\Phi_1 > \Phi_2 \tag{89}$$

Proof: According to (30), when M is odd, the number of consecutive lags of the non-negative co-array can be expressed as

$$\Phi_1 = Q + M(Q - N) + \frac{1}{2}(M + 1)(Q - M). \tag{90}$$

Swapping M and N, the number of consecutive lags of the non-negative co-array is given by

$$\Phi_2 = Q + (Q - N)M + \frac{1}{2}M(Q - M). \tag{91}$$

Obviously, $\Phi_1 > \Phi_2$. ■

When Q is even, because M and N are coprime, M and N must be odd. Combining *Lemma 1*, Combining Lemma 1, we can conclude that whether Q is odd or even, in order to obtain a larger Φ, M must be odd. Therefore, we have $\Phi = MN + M + N + (M + 1)N/2$.

Let $N = Q - M$, the optimization problem in (31) can be rewritten as

$$\max \quad \left(-\frac{3}{2}M^2 + \left(\frac{3}{2}Q - \frac{1}{2}\right)M + \frac{3}{2}Q \right). \tag{92}$$

Differentiating the above equation w.r.t M and equating to zero, we obtain

$$\widetilde{M}_{opt} = \frac{1}{2}Q - \frac{1}{6}. \tag{93}$$

Because M is odd and $\widetilde{M}_{opt}$ is not an integer, we need to find the odd number closest to $\widetilde{M}_{opt}$. We discuss it separately according to the parity of Q.

When Q is even and $Q/2$ is odd and closest to $\widetilde{M}_{opt}$, we obtain $M = N = Q/2$, which is in contradiction with the coprimality of M and N. Therefore, the optimum value of M, N is given by

$$M_{opt} = \frac{Q}{2} - 2, N_{opt} = \frac{Q}{2} + 2. \tag{94}$$

When Q is even and $Q/2$ is even, the odd closest to $\widetilde{M}_{opt}$ is $Q/2 - 1$. Therefore, the optimum value of M, N is given by

$$M_{opt} = \frac{Q}{2} - 1, N_{opt} = \frac{Q}{2} + 1. \tag{95}$$

When Q is odd and $(Q+1)/2$ is even, the odd closest to $\widetilde{M}_{opt}$ is $(Q-1)/2$. Therefore, the optimum value of M, N is given by

$$M_{opt} = \frac{Q-1}{2}, N_{opt} = \frac{Q+1}{2}. \tag{96}$$

When Q is even and $Q/2$ is even, the odd closest to $\widetilde{M}_{opt}$ is $(Q+1)/2$. Therefore, the optimum value of M, N is given by

$$M_{opt} = \frac{Q+1}{2}, N = \frac{Q-1}{2}. \tag{97}$$

Submitting these (94)-(97) to (31), we get the equation (33). ■

APPENDIX D
PROOF OF PROPOSITION 4

According to [34], we obtain the $w(l)$ easily when $l \notin \pm\mathbb{D}_{1,2}$. Here, we give the proof of the weight function when $l \in \pm\mathbb{D}_{1,2}$ only. As described as (22), $\mathbb{D}_{1,2} = \{mN - nM - L | 0 \leq m \leq M, 1 \leq n \leq N-1\}$ and $\mathbb{D}_{1,2} = -\mathbb{D}_{2,1}$.

First, we prove that there are $(M+1)(N-1)$ unique lags in $\mathbb{D}_{1,2}$. If there exists two the same lags, we obtain

$$\begin{aligned} m_1N - n_1M - L &= m_2N - n_2\text{M-L} \\ \Rightarrow \frac{n_1 - n_2}{m_1 - m_2} &= \frac{N}{M}, \end{aligned} \tag{98}$$

where $0 \leq m_1, m_2 \leq M$ and $1 \leq n_1, n_2 \leq N-1$. Because of $n_1 - n_2 < N$ and the coprimality of M and N, the equation (98) doesn't hold. Therefore, there are no duplicate elements in $\mathbb{D}_{1,2}$, i.e. $(M+1)(N-1)$ unique lags.

Next, we prove that, when $L = (M+1)N/2$, there not exists the same lags between $\mathbb{D}_{1,2}$ and $\mathbb{D}_{2,1}$. If there exists the same lags between the two sets, the equation

$$m_1N - n_1M - L = n_2M + L - m_2N \tag{99}$$

holds, where $0 \leq m_1, m_2 \leq M$ and $1 \leq n_1, n_2 \leq N-1$. Substituting $L = (M+1)N/2$ into (99) gives

$$\frac{m_1 + m_2 - M - 1}{n_1 + n_2} = \frac{M}{N}. \tag{100}$$

Since $m_1 + m_2 - M - 1 < M$ and the coprimality of M and N, we cannot find the integers m_1 that satisfies (100). ■

ACKNOWLEDGMENT

The authors declare that they have no conflicts of interest, and they confirm that the funding did not lead to any conflict of interests regarding the publication of this manuscript. The authors claim that the data used in this article are provided by our simulations and this is developed without using any data in a published article to support our results.

REFERENCES

[1] H. Krim and M. Viberg, "Two decades of array signal processing research: The parametric approach," *IEEE Signal Process. Mag.*, vol. 13, no. 4, pp. 67–94, Jul. 1996.

[2] A. Hero, H. Messer, J. Goldberg, and D. Thomson, "Highlights of statistical signal and array processing," *IEEE Signal Process. Mag.*, vol. 15, no. 5, pp. 21–64, Sep. 1998.

[3] P. Zetterberg and B. Ottersten, "The spectrum efficiency of a base station antenna array system for spatially selective transmission," *IEEE Trans. Veh. Technol.*, vol. 44, no. 3, pp. 651–660, Aug. 1995.

[4] P. Stoica and N. Arye, "MUSIC, maximum likelihood, and Cramer-Rao bound," *IEEE Trans. Acoust., Speech Signal Process.*, vol. 37, no. 5, pp. 720–741, May 1989.

[5] R. Roy and T. Kailath, "Esprit-estimation of signal parameters via rotational invariance techniques," *IEEE Trans. Acoust., Speech, Signal Process.*, vol. 37, no. 7, pp. 984–995, Jul. 1989.

[6] A. Moffet, "Minimum-redundancy linear arrays," *IEEE Trans. Antennas Propag.*, vol. AP-6, no. 2, pp. 172–175, Mar. 1968.

[7] P. Pal and P. P. Vaidyanathan, "Nested arrays: A novel approach to array processing with enhanced degrees of freedom," *IEEE Trans. Signal Process.*, vol. 58, no. 8, pp. 4167–4181, Aug. 2010.

[8] P. P. Vaidyanathan and P. Pal, "Sparse sensing with co-prime samplers and arrays," *IEEE Trans. Signal Process.*, vol. 59, no. 2, pp. 573–586, Feb. 2011.

[9] P. Pal and P. P. Vaidyanathan, "Coprime sampling and the music algorithm," *Proc. Digit. Signal Process. Signal Process. Educ. Meeting (DSP/SPE)*, 2011, pp. 289–294.

[10] Y. D. Zhang, M. G. Amin, and B. Himed, "Sparsity-based DOA estimation using co-prime arrays," in *Proc. IEEE Int. Conf. Acoust., Speech Signal Process.*, May 2013, pp. 3967–3971.

[11] Q. Shen, W. Liu, W. Cui, and S. Wu, "Underdetermined DOA estimation under the compressive sensing framework: A review," *IEEE Access*, vol. 4, pp. 8865–8878, 2016.

[12] Q. Shen, W. Cui, W. Liu, S. Wu, Y. D. Zhang, and M. G. Amin, "Underdetermined wideband DOA estimation of off-grid sources employing the difference co-array concept," *Signal Process.*, vol. 130, no. 1, pp. 299–304, 2017.

[13] S. Qin, Y. D. Zhang, and M. G. Amin, "Generalized coprime array configurations for direction-of-arrival estimation," *IEEE Trans. Signal Process.*, vol. 63, no. 6, pp. 1377–1390, Mar. 2015

[14] C.-L. Liu and P. P. Vaidyanathan, "Super nested arrays: Linear sparse arrays with reduced mutual coupling—Part I: Fundamentals," *IEEE Trans. Signal Process.*, vol. 64, no. 15, pp. 3997–4012, Aug. 2016.

[15] J. Liu, Y. Zhang, Y. Lu, S. Ren, and S. Cao, "Augmented nested arrays with enhanced DOF and reduced mutual coupling," *IEEE Trans. Signal Process.*, vol. 65, no. 21, pp. 5549–5563, Nov. 2017.

[16] Z. Zheng, W.-Q. Wang, Y. Kong, and Y. D. Zhang, "MISC array: A new sparse array design achieving increased degrees of freedom and reduced mutual coupling effect," *IEEE Trans. Single Process.*, vol. 67, no. 7, pp. 1728–1741, Apr. 2019.

[17] P. Chargé, Y. Wang, and J. Saillard, "A non-circular sources direction finding method using polynomial rooting," *Signal Process.*, vol. 81, no. 8, pp. 1765–1770, 2001.

[18] M. Haardt and F. Romer, "Enhancements of unitary esprit for non-circular sources," in *Proc. IEEE Int. Conf. Acoust., Speech, Signal Process.*, vol. 2, May 2004, p. 101.

[19] H. Abeida and J.-P. Delmas, "MUSIC-like estimation of direction of arrival for noncircular sources," *IEEE Trans. Signal Process.*, vol. 54, no. 7, pp. 2678–2690, Jul. 2006.

[20] J. Liu, Z. Huang, and Y. Zhou, "Extended 2q-MUSIC algorithm for noncircular signals," *Signal Process.*, vol. 88, no. 6, pp. 1327–1339, Jun. 2008.

[21] H. Abeida and J. P. Delmas, "Statistical performance of MUSIC-like algorithms in resolving noncircular sources," *IEEE Trans. Signal Process.*, vol. 56, no. 9, pp. 4317–4329, Sep. 2008.

[22] F. Gao, A. Nallanathan, and Y. Wang, "Improved MUSIC under the coexistence of both circular and noncircular sources," *IEEE Trans. Signal Process.*, vol. 56, no. 7, pp. 3033–3038, Jul. 2008.

[23] Z. T. Huang, Z. M. Liu, J. Liu, and Y. Y. Zhou, "Performance analysis of MUSIC for non-circular signals in the presence of mutual coupling," *IET Radar, Sonar Navigat.*, vol. 4, no. 5, pp. 703–711, 2010.

[24] X. Yang, G. Li, and Z. Zheng, "DOA estimation of noncircular signal based on sparse representation," *Wireless Pers. Commun.*, vol. 82, no. 4, pp. 2363–2375, 2015.

[25] J. Cai, W. Liu, R. Zong, and B. Wu, "Sparse array extension for non-circular signals with subspace and compressive sensing based DOA estimation methods," *Signal Process.*, vol. 145, pp. 59–67, Apr. 2018.

[26] Y. Wang, M. Trinkle, and B. W.-H. Ng, "Efficient DOA estimation of noncircular signals in the presence of multipath propagation," *Signal Process.*, vol. 149, pp. 14–26, Aug. 2018.

[27] X. Wang, Z. Chen, S. Ren, and S. Cao, "DOA estimation based on the difference and sum coarray for coprime arrays," *Digit. Signal Process.*, vol. 69, pp. 22–31, Oct. 2017.
[28] Z. Chen, Y. Ding, S. Ren, and Z. Chen, "A novel noncircular MUSIC algorithm based on the concept of the difference and sum coarray," *Sensors*, vol. 18, no. 2, p. 344, Jan. 2018.
[29] P. Gupta and M. Agrawal, "Design and analysis of the sparse array for DOA estimation of noncircular signals," *IEEE Trans. Signal Process.*, vol. 67, no. 2, pp. 460–473, Jan. 2019.
[30] Y. Wang, W. Wu, X. Zhang, and W. Zheng, "Transformed nested array designed for DOA estimation of non-circular signals: Reduced sum-difference co-array redundancy perspective," *IEEE Commun. Lett.*, vol. 24, no. 6, pp. 1262–1265, Jun. 2020.
[31] W. Si, F. Zeng, C. Zhang, and Z. Peng, "Improved coprime arrays with reduced mutual coupling based on the concept of difference and sum coarray," *IEEE Access*, vol. 7, pp. 66251–66262, 2019.
[32] J. R. M. Neudecker, "The commutation matrix: Some properties and applications," *Ann. Statist.*, vol. 7, no. 2, pp. 381–394, 1979.
[33] C.-L. Liu and P. P. Vaidyanathan, "Cramér–Rao bounds for coprime and other sparse arrays, which find more sources than sensors," *Digit. Signal Process.*, vol. 61, pp. 43–61, Feb. 2017.
[34] U. V. Dias and S. Srirangarajan, "Co-prime arrays and difference set analysis," in *Proc. 25th Eur. Signal Process. Conf. (EUSIPCO)*, Aug. 2017, pp. 931–935.

FENGTONG MEI was born in 1985. He received the B.S. degree from the National Digital Switching System Engineering and Technological Research Center (NDSC), Zhengzhou, China, in June 2009, and the M.S. degree from Zhengzhou University, Zhengzhou, in June 2016. He is currently pursuing the Ph.D. degree in communications and information system with NDSC. His main research interests include wireless communication theory, signal processing, and parameter estimation.

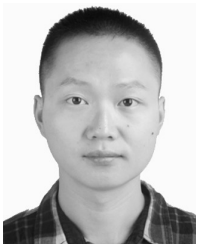

HAIYUN XU received the M.S. degree from the National Digital Switching System Engineering and Technological Research Center (NDSC), Zhengzhou, China, in June 2019, where he is currently pursuing the Ph.D. degree in communications and information system. His main research interests include array signal processing and wireless communication.

WEIJIA CUI was born in 1976. He is currently a Professor with the National Digital Switching System Engineering and Technological Research and Development Center (NDSC), Zhengzhou, China. His main research interests include signal processing and intelligent information processing.

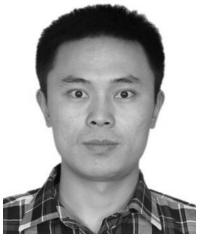

BIN BA was born in 1987. He received the M.S. and Ph.D. degrees from the National Digital Switching System Engineering and Technological Research Center (NDSC), Zhengzhou, China, in June 2012 and June 2015, respectively. He is currently working in communications and information system with NDSC. His main research interests include wireless communication theory, signal processing, and parameter estimation.

YINSHENG WANG was born in 1990. He received the M.S. degree from Chengdu University of Technology, Chengdu, China, in 2017. He is currently pursuing the Ph.D. degree in communications and information system with the National Digital Switching System Engineering and Technological Research Center (NDSC). His main research interests include array signal processing and wireless communication.